Journal of Biomedical Optics

SPIEDigitalLibrary.org/jbo

Photoacoustic resonance spectroscopy for biological tissue characterization

Fei Gao
Xiaohua Feng
Yuanjin Zheng
Claus-Dieter Ohl

SPIE

Photoacoustic resonance spectroscopy for biological tissue characterization

Fei Gao,[a] Xiaohua Feng,[a] Yuanjin Zheng,[a,*] and Claus-Dieter Ohl[b]
[a]Nanyang Technological University, School of Electrical and Electronic Engineering, 50 Nanyang Avenue, 639798 Singapore
[b]Nanyang Technological University, School of Physical and Mathematical Sciences, 50 Nanyang Avenue, 639798 Singapore

Abstract. By "listening to photons," photoacoustics allows the probing of chromosomes in depth beyond the optical diffusion limit. Here we report the photoacoustic resonance effect induced by multiburst modulated laser illumination, which is theoretically modeled as a damped mass-string oscillator and a resistor-inductor-capacitor (RLC) circuit. Through sweeping the frequency of multiburst modulated laser, the photoacoustic resonance effect is observed experimentally on phantoms and porcine tissues. Experimental results demonstrate different spectra for each phantom and tissue sample to show significant potential for spectroscopic analysis, fusing optical absorption and mechanical vibration properties. Unique RLC circuit parameters are extracted to quantitatively characterize phantom and biological tissues. [DOI: 10.1117/1.JBO.19.6.067006]

Keywords: photoacoustic; resonance; spectroscopy; characterization.

Paper 140153R received Mar. 6, 2014; revised manuscript received May 6, 2014; accepted for publication May 19, 2014; published online Jun. 13, 2014.

1 Introduction

The term photoacoustics summarizes thermoelastically generated acoustic emission due to the absorption of light.[1–4] In recent years, photoacoustic microscopy (PAM) and photoacoustic tomography (PAT) have been applied to multiscale studies from subcutaneous vasculature microscopic imaging to whole-body small-animal imaging *in vivo*. Both give simultaneously high optical contrast and high acoustic resolution, as they are not limited by optical diffusion.[5] Functional PA imaging has been proposed to detect the wavelength-dependent property of optical absorbers, which leads to important applications such as oxygen saturation detection and imaging.[6–13] From the physical perspective, the PA effect is a hybrid physical process involving both optical absorption and mechanical vibrations. Unfortunately, almost all the state-of-art PAM/PAT systems only exploit the optical absorption feature while ignoring the mechanical response of the biological tissue. Sensing the resonance of the biological tissue may result in enhanced endogenous contrast. In this work, we report on photoacoustic resonance (PAR) of biological tissues induced by multiburst modulated laser illumination. PAR spectroscopy may allow characterization/identification of tissues through their mechanical properties, resonance frequency, and damping factor.

2 Theory of PAR Spectroscopy

A good overview on techniques and modeling is available in two review articles.[1,2] In short, biological tissue illuminated with an intensity-modulated laser will experience optical energy absorption, localized heating, and thermal expansion [see Fig. 1(a)]. Modeling a small enough viscid biological tissue as an ideal point source,[14–16] the acoustic pressure emitted, $p(t)$, follows the expression

$$\frac{\partial^2}{\partial t^2}p(t)+a^2\frac{\xi+\frac{4}{3}\eta}{\rho}\frac{\partial}{\partial t}p(t)+a^2c^2p(t)=\Gamma\frac{\partial H(t)}{\partial t}, \quad (1)$$

where a is the propagation phase constant, ρ is the tissue density, η is the shear viscosity, ξ is the bulk viscosity, and c is the speed of sound in the tissue. Γ is the Grüneisen constant expressed as $\Gamma=\beta c^2/c_p$, where β is the thermal expansion coefficient and c_p is the constant pressure heat capacity per unit mass. $H(t)=\mu_a\Phi(t)$ is the heating function from the laser illumination, where μ_a is the optical absorption coefficient of the tissue and $\Phi(t)$ is the optical fluence rate. Equation (1) is applicable when the sample is homogeneous and the light illumination is uniform, which are well controlled in the phantom experiments below.

Equation (1) is a second-order differential pressure equation driven by the source term $\Gamma\times\partial H(t)/\partial t$. Therefore, we propose to rewrite Eq. (1) as a damped mass-string oscillator model[17] [see Fig. 1(b)]. Here we introduce the coordinate $x(t)$ to describe the displacement of the mass m of this oscillator, resulting in

$$\frac{\partial^2}{\partial t^2}x(t)+\frac{b}{m}\frac{\partial}{\partial t}x(t)+\frac{k}{m}x(t)=\frac{F(t)}{m}. \quad (2)$$

In Eq. (2), k is the spring constant and b is the damping coefficient. Without losing generality, we assume that the driving force term follows a cosine wave $F(t)/m=f_0\cos(\omega t)$; the steady-state displacement is given by

$$x(t)=A\cos(\omega t-\theta), \quad (3)$$

where θ is the phase shift between the displacement and the driving force, and A is the magnitude expressed as

*Address all correspondence to: Yuanjin Zheng, E-mail: yjzheng@ntu.edu.sg

0091-3286/2014/$25.00

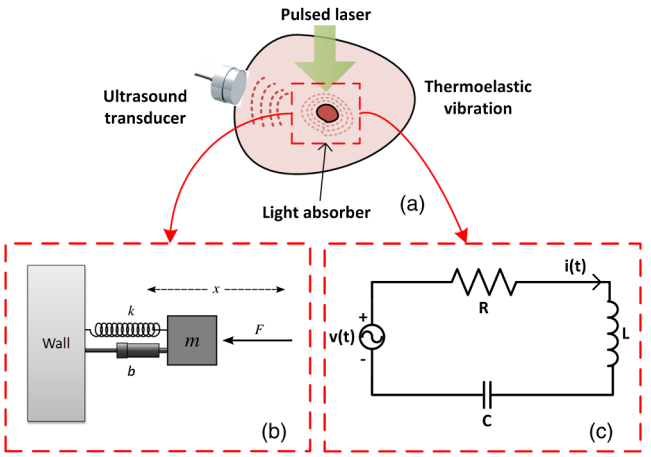

Fig. 1 (a) Diagram of photoacoustic effect induced by laser illumination. (b) The equivalent mass-string damped oscillator model driven by force F. (c) Equivalent resistor-inductor-capacitor circuit model.

$$A = \frac{f_0}{\sqrt{\left(\frac{k}{m} - \omega^2\right)^2 + \left(\frac{b}{m}\omega\right)^2}}. \tag{4}$$

The maximum displacement will be reached at the resonance frequency ω_0.

$$\omega_0 = \sqrt{\frac{k}{m} - \frac{1}{2}\left(\frac{b}{m}\right)^2}. \tag{5}$$

Converting the damped mass-string oscillator model back into the PA pressure equation [Eq. (1)], we expect that the magnitude of PA signal will be largest at its resonance frequency. We term this condition PAR. From the equivalence of Eqs. (1) and (2), we obtain

$$\frac{1}{m} = \Gamma, \quad \frac{b}{m} = a^2\frac{\xi + \frac{4}{3}\eta}{\rho}, \quad \frac{k}{m} = a^2c^2, \tag{6}$$

and then the resonance frequency of biological tissue is

$$\omega_{\text{tissue}} = \sqrt{a^2c^2 - \frac{1}{2}\left(a^2\frac{\xi + \frac{4}{3}\eta}{\rho}\right)^2}, \tag{7}$$

with a quality factor of

$$Q = \frac{m}{b}\omega_{\text{tissue}} = \sqrt{\frac{\rho^2c^2}{a^2\left(\xi + \frac{4}{3}\eta\right)^2} - \frac{1}{2}}. \tag{8}$$

Similarly, the PAR effect can also be modeled as a resistor-inductor-capacitor (RLC) circuit as shown in Fig. 1(c), following the second-order differential equation

$$\frac{\partial^2}{\partial t^2}i(t) + \frac{R}{L}\frac{\partial}{\partial t}i(t) + \frac{1}{LC}i(t) = \frac{1}{L}\frac{\partial}{\partial t}v(t). \tag{9}$$

Then the parameters could be mapped from the mechanical oscillator to the RLC circuit.

$$\frac{R}{L} = \frac{b}{m}, \quad \frac{1}{LC} = \frac{k}{m}, \quad \frac{1}{L} = \frac{1}{m}. \tag{10}$$

Now we have modeled the PAR effect as both the mass-string oscillator and the RLC circuit model. It is observed that tissues with different mechanical properties, such as acoustic velocity and viscosity, etc., will exhibit different resonance frequencies and quality factors. Therefore, by sweeping the frequency of a multiburst modulated laser beam, the PA response of different tissues could be maximized when the frequency hits their unique resonance frequencies. This technique is named PAR spectroscopy. Moreover, different kinds of biological tissues may be modeled by parallel and/or serial circuits to obtain an effective impedance and phase.

3 Experimental Results

The experimental setup for PAR effect and PAR spectroscopy studies is shown in Fig. 2(a): a continuous-wave (CW) laser (RD532-100G4, Laser-rich Ltd., Xi'an, Shaanxi, China) with 1-W average power and 532-nm wavelength is used to provide the light source, which is focused by a condenser lens (LB1471, Thorlabs, Newton, New Jersey) and fed into an acousto-optic modulator (AOM) (R23080-1-.85-LTD, Gooch & Housego, Ilminster Somerset, United Kingdom) for intensity modulation controlled by a function generator (33250A, Agilent, Santa Clara, California). The function generator provides multiburst waveform with its frequency swept for spectrum analysis. A beam splitter and a photodiode (DET10A, Thorlabs) are used to monitor the input laser power for calibration purposes. The laser beam is weakly focused by a condenser lens (4-cm focal length) onto the center of biological tissue placed in de-ionized water with a spot of ~2 mm diameter. The tissue samples are wrapped by a very thin polyethylene film for isolation to avoid water dilution. The wrapped tissue samples are attached to the bottom of the water tank using double-faced adhesive tape to avoid tissue movement. The photoacoustic signal is collected by a wideband ultrasound transducer placed 1 cm away from the sample with 2.25-MHz central frequency (fractional bandwidth: 60%, V323-SU, Olympus, Tokyo, Japan) mounted on an X-Y stage for position adjustment, followed by an ultrasound preamplifier (Model 5662, Olympus). A digital oscilloscope (HDO4000, 12-bit, Lecroy, Chestnut Ridge, New York) is used to record the PA signal at 500-MHz sampling rate. The photograph of the experimental setup is shown in Fig. 2(b), as well as a typical modulated laser light pattern appended in Fig. 2(c). The intensities of the modulated laser output are relatively constant around 0.2 W in the frequency range of 50 to 150 kHz, indicating the AOM modulation efficiency to be ~20%.

To prove the PAR effect and the feasibility of the proposed PAR spectroscopy, three agar phantoms with different agar concentrations (1, 2, and 3%) are prepared to simulate tissues with different mechanical properties, such as viscosity and acoustic impedance, which are made into slices of 3-mm thickness. By sweeping the multiburst modulation frequency of the laser source from 50 to 150 kHz with steps of 2 kHz, the peak-to-peak amplitude of the PA signal is calculated and recorded at every frequency point to construct the PAR spectrum. The resonance frequency ω_0 and −3-dB bandwidth Δf could be obtained by the frequency where amplitude reaches maximum and the frequency difference where the amplitude drops by −3 dB, respectively. Then the quality factor Q could be

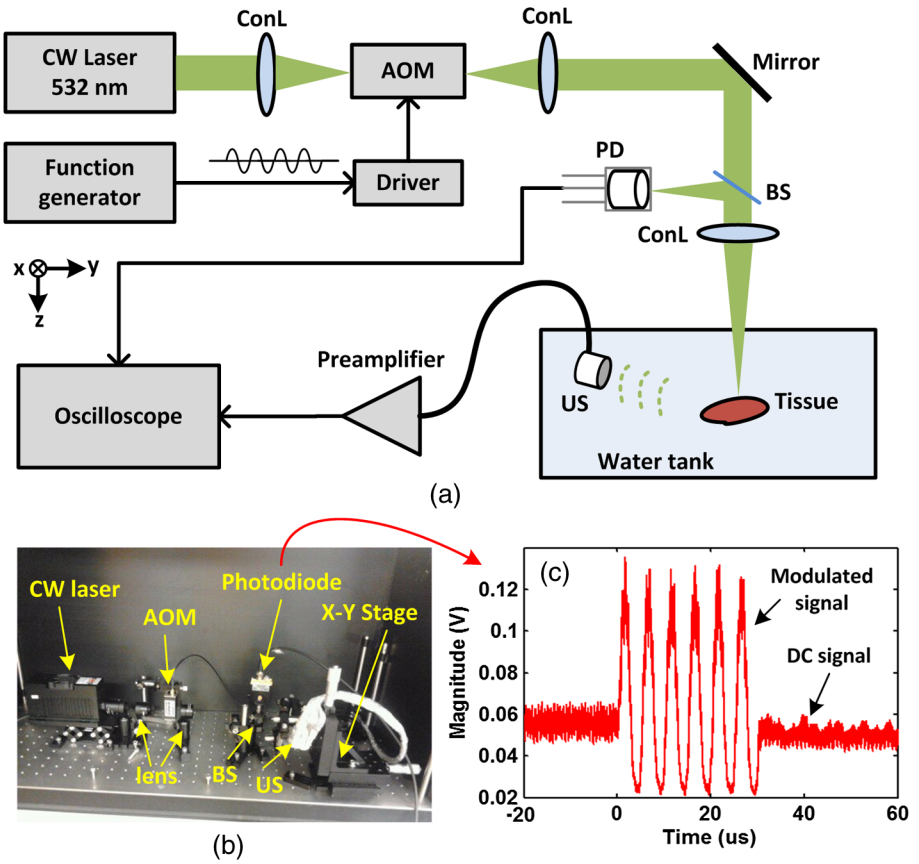

Fig. 2 (a) Diagram of the experimental setup for the observation of photoacoustic resonance effect and spectroscopy. ConL, condenser lens; AOM, acousto-optic modulator; BS, beam splitter; PD, photodiode; US, ultrasound transducer. (b) The photograph of the experimental setup. (c) A typical modulated laser light pattern.

quantified by $Q = \omega_0/\Delta f$. Utilizing an ultrasound transducer with a flat frequency response in the covered band, the spectra of the three phantoms are shown in Fig. 3(a), where a clear resonance is found in each phantom, demonstrating the PAR effect. In addition, phantoms with higher agar concentration (higher viscosity) exhibit lower resonance frequency, which matches with the prediction from Eq. (7). The waveforms of the PA signals from phantom 3 at resonance (75 kHz) and nonresonance (130 kHz) are shown in Fig. 3(b), where the PA signal at resonance has increasingly larger amplitude (>0.8 mV) and significantly narrower bandwidth of <20 kHz (high Q) than the PA signal at nonresonance with amplitude <0.4 mV and bandwidth >200 kHz (low Q), as expected.

To further verify the feasibility of PAR spectroscopy for tissue characterization, three kinds of porcine tissues (muscle, fat, liver) are prepared in slices to be tested by the PAR spectroscopy by sweeping the multiburst modulation frequency from 50 to 300 kHz. Figure 3(c) shows that the liver has the lowest

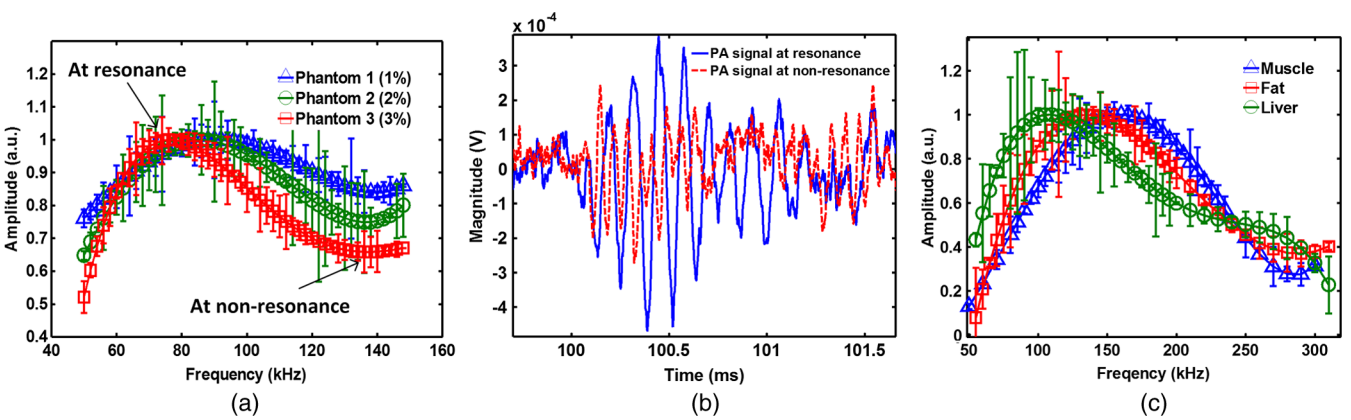

Fig. 3 (a) The photoacoustic resonance (PAR) spectroscopy for three phantoms with different agar densities to simulate the different mechanical properties. (b) Waveforms of photoacoustic signal at resonance and nonresonance. (c) PAR spectroscopy for three different biological tissues characterized by their resonance frequencies and Q factors.

resonance frequency due to its highest viscosity, while muscle has the highest resonance frequency with smallest viscosity, which is matched well with previously reported data.[18] Repeated experiments (10 times) lead to variations and are stated as error bars in Fig. 3. The variations may be caused by different sample positioning variation, geometry variation of the samples, nonuniform heating of the samples, and ultrasound detection distance fluctuation. Nevertheless PAR spectroscopy provides distinguishable mechanical resonance properties for different biological tissues, showing the potential to achieve a new kind of spectroscopic imaging. It is worth noting that the PA generation efficiency is generally proportional to the modulation frequency of the CW laser excitation, which could be the main reason of the asymmetric response around the resonance frequency in Figs. 3(a) and 3(c). Within a relatively narrow bandwidth around the resonance frequency for PAR spectroscopy, the PA amplitude almost does not change with the modulation frequency. Therefore, this variation of PA generation efficiency caused by the modulation frequency may induce some distortion on the PAR spectroscopy (e.g., asymmetric spectrum response); however, it will not influence the characterization capability of PAR spectroscopy, where the resonance frequency and quality factor could be extracted from the asymmetric PAR spectrum.

Next we will extract the RLC circuit parameters and impedance from the resonance frequency and quality factor shown in the spectra shown in Figs. 3(a) and 3(c). Based on Eqs. (6) and (10), $L = 1/\Gamma$, where the Grüneisen factor Γ is normally supposed to be constant for all the samples, so here the inductance is chosen to be 1 H for normalization. Then according to the resonance frequency ω_0 and quality factor Q exacted from the PAR spectrums, R, L, and C can be calculated from the extracted ω_0 and Q with the following equations by substituting Eq. (10) into Eqs. (6) to (9):

$$R = \omega_0 L\sqrt{2Q^2-1}, \quad C = \frac{2Q^2}{\omega_0^2 L(2Q^2+1)}, \quad L = 1. \tag{11}$$

Based on Eq. (11), the circuit complex impedance $Z = R + j\omega_0 L + 1/j\omega_0 C$ can be calculated. Now the different phantoms and porcine tissues have been quantitatively characterized by the equivalent RLC circuit parameters. It is worth noting that for different phantoms and tissue samples, the absolute values of real part and imaginary part of the circuit impedance are changing in opposite ways, i.e., when the real part is decreasing, the imaginary part is increasing, and vice versa. Therefore, similar to the recently proposed concept of phasoscopy,[19] we can employ the phase $\tan\varphi = \mathrm{Im}(Z)/\mathrm{Re}(Z)$ of the circuit impedance as for PAR spectroscopy characterization. As described above, R, L, C, ω_0, Q, Z, and $\tan\varphi$ of the phantoms and tissues are listed in Table 1. The mechanical properties of the samples could be readily derived from Eqs. (7) and (8) by substituting the quantified resonance frequency ω_0 and quality factor Q with some calibration in advance. Furthermore, the extracted phase can be derived from Eqs. (6) to (10) as

$$\begin{aligned}\tan\varphi &= \left[\sqrt{a^2c^2 - \frac{1}{2}\left(a^2\frac{\xi+\frac{4}{3}\eta}{\rho}\right)^2}\right]\left[\frac{\rho(\xi+\frac{4}{3}\eta)}{a^2(\xi+\frac{4}{3}\eta)^2 - 2\rho^2c^2}\right] \\ &= \left(\frac{-\frac{1}{2}\Lambda}{\sqrt{1-\frac{1}{2}\Lambda^2}}\right), \quad \text{where } \Lambda = a\frac{\xi+\frac{4}{3}\eta}{\rho c}.\end{aligned} \tag{12}$$

If we choose negative a with $|a| \ll 1$, then Eq. (12) can be approximated as

$$\tan\varphi \approx -\frac{1}{2}\left(\Lambda + \frac{1}{4}\Lambda^3\right) \approx -\frac{1}{2}\Lambda. \tag{13}$$

Equation (13) reveals that the proposed spectroscopy indicator $\tan\varphi$ is the ratio between viscosity parameter, $\xi + 4/3\eta$, and acoustic impedance, ρc, fusing the viscosity imaging and ultrasound imaging to achieve an improved contrast.

4 Discussion and Conclusion

The advantage of the proposed PAR spectroscopy is threefold. First, from the physical perspective, compared with conventional PA approaches exploring the optical absorption property of biological tissues only, the proposed PAR spectroscopy based on the PAR effect is revealing both optical absorption and mechanical resonance properties, which is intrinsically an endogenous dual-contrast characterization approach. In addition, separation of the two kinds of contrasts is also feasible: PA mechanical resonance spectrum in terms of resonance frequency (ω_0) and quality factor (Q) is related with mechanical property only (viscosity, mechanical impedance), and does not depend on optical absorption property. On the other hand, optical absorption contrast could also be readily obtained by utilizing single-pulse modulation of the CW laser source, which is similar to pulsed laser illumination without resonating

Table 1 Resistor-inductor-capacitor circuit parameters of three phantoms and porcine tissues.

Sample	ω_0 (kHz)	Q	R (kΩ)	C (pF)	L (H)	$Z(\Omega)$	$\tan\varphi\|_{\omega=\omega_0}$
Phantom 1	90	0.5	71.59	93.787	1	$7.159\times10^4 + j\omega(0.1188)$	0.1825
Phantom 2	85	1.1	67.61	105.14	1	$6.761\times10^4 + j\omega(0.2140)$	0.3482
Phantom 3	73	1.5	58.07	142.55	1	$5.807\times10^4 + j\omega(0.4203)$	0.7961
Muscle	160	1.4	127.27	29.675	1	$1.2727\times10^5 + j\omega(0.1575)$	0.2476
Fat	130	1.2	103.41	44.951	1	$1.0341\times10^5 + j\omega(0.4438)$	0.8584
Liver	110	1.0	87.50	62.783	1	$8.750\times10^4 + j\omega(0.6018)$	1.3756

the biological tissue. Second, from the performance perspective, utilizing the PAR effect, the PA signal of the object could be maximized at its resonance frequency to enhance the SNR within a narrow bandwidth around the resonance frequency of the PAR spectrum, where the PA generation efficiency variation has negligible influence. In addition, the narrowband characteristic of the PA signal at resonance allows subsequent narrowband amplification and detection using lock-in amplifier with much higher sensitivity than conventional wideband PA signals induced by single-pulse lasers.[20,21] Third, from the application perspective, potential applications of PAR spectroscopy will extend the conventional PAM/PAT applications. The proposed PAR spectroscopy is also capable of revealing the mechanical resonance properties related with viscosity and acoustic impedance, which are also important indicators of biological tissue and other materials.[22,23] In brief, the PAR effect and spectroscopy proposed in this paper are a marriage of optical absorption and mechanical resonance effects, going beyond conventional pulsed-laser PA approaches by providing endogenous dual-contrast performance.

Compared with the conventional ultrasound imaging to quantify the mechanical properties, the proposed PAR approach has two distinct advantages: to enable a typical PAT system to perform ultrasound imaging, extra ultrasound transmitter modules are needed for beamforming that incur high power amplification, which could increase the total system cost and complexity of PAT. On the other hand, the proposed PAR approach does not need the ultrasound transmitter modules, achieving relatively lower system cost and complexity. More interestingly, the PAR approach is receiving the PA signals only from the object to extract both optical absorption and mechanical vibration properties, which are intrinsically correlated with the exact same object. However, if using another ultrasound imaging to acquire the mechanical property of the object, the ultrasound imaging and PA imaging are performed separately, leading to potential mismatch on the characterization of the same object. Although overlapped PA and ultrasound images could be obtained in some research groups[24] and companies (VisualSonics Inc., Toronto, Ontario, Canada), they only give a separate PA image characterizing the optical absorption and a B-mode ultrasound image characterizing the acoustic impedance mismatch of the tissue, where the correlation between the PA and ultrasound are not fully explored. These problems could potentially be solved by the proposed PAR approach in this paper.

The disadvantages associated with the proposed PAR spectroscopy may include the following. PAR spectroscopy requires a CW laser, which has much lower peak power than the pulsed laser, resulting in low signal SNR. High-sensitivity lock-in detection and more data averaging are needed, which may induce higher system cost and longer data acquisition time. Moreover, the AOM modulation will further increase the system complexity and decrease the output laser energy compared with pulsed laser PA systems. These disadvantages could be potentially overcome by employing higher-power CW laser and dedicated low-noise amplifier. Moreover, a chirp-modulated CW laser source could be utilized to improve the signal SNR by matched filter processing through cross-correlating the received PA signal with a reference chirp signal, which has shown comparable signal SNR with pulsed laser-based PAT.[25,26] Another similar technique is coded excitation–based PA imaging by encoding the laser diode excitation in a frequency-chirping manner.[27] More interestingly, the above chirp-based laser excitation techniques could also be utilized for the proposed PAR spectroscopy in real time, directly by selecting proper chirping frequency range and duration time, which will be studied in future.

Although the PA point source generation [Eq. (1)] could explain the PAR spectroscopy concept and the phantom experiments very well in this paper, a more detailed PA generation modeling will be needed, especially for highly heterogeneous biological tissues with nonuniform thermal coupling. A recent preliminary study of complex circuit modeling of thermoacoustic generation is referred to in Refs. 28 and 29. As a proof-of-concept work, we have proposed PA resonance spectroscopy to characterize different kinds of phantoms or tissues in a qualitative manner, validating its potential for biomedical sensing and imaging. The accurate and quantitative calculation of the real viscosity and acoustic impedance values from the PAR spectra will be thoroughly studied in future work to push the proposed PAR spectroscopy for more accurate tissue properties quantization.

In summary, the PAR effect is modeled with a damped mass-string oscillator model and an equivalent RLC electrical circuit model, and investigated experimentally by sweeping the multi-burst modulation frequency of the CW laser source. Both agar phantoms and biological tissues are tested to demonstrate the effect of mechanical tissue properties. Currently, we are developing a PAR imaging technique to be implemented for *in vivo* animal studies.

Acknowledgments

This research is supported by the Singapore National Research Foundation under its Exploratory/Developmental Grant (NMRC/EDG/1062/2012) and administered by the Singapore Ministry of Health's National Medical Research Council.

References

1. M. H. Xu and L. H. V. Wang, "Photoacoustic imaging in biomedicine," *Rev. Sci. Instrum.* **77**(4), 041101 (2006).
2. A. C. Tam, "Applications of photoacoustic sensing techniques," *Rev. Mod. Phys.* **58**(2), 381–431 (1986).
3. X. D. Wang et al., "Noninvasive laser-induced photoacoustic tomography for structural and functional in vivo imaging of the brain," *Nat. Biotechnol.* **21**(7), 803–806 (2003).
4. H. F. Zhang, K. Maslov, and L. H. V. Wang, "*In vivo* imaging of subcutaneous structures using functional photoacoustic microscopy," *Nat. Protoc.* **2**(4), 797–804 (2007).
5. L. H. V. Wang and S. Hu, "Photoacoustic tomography: in vivo imaging from organelles to organs," *Science* **335**(6075), 1458–1462 (2012).
6. H. F. Zhang et al., "Functional photoacoustic microscopy for high-resolution and noninvasive *in vivo* imaging," *Nat. Biotechnol.* **24**(7), 848–851 (2006).
7. B. Cox et al., "Quantitative spectroscopic photoacoustic imaging: a review," *J. Biomed. Opt.* **17**(6), 061202 (2012).
8. D. Razansky et al., "Multispectral opto-acoustic tomography of deep-seated fluorescent proteins in vivo," *Nat. Photonics* **3**(7), 412–417 (2009).
9. L. V. Wang, "Multiscale photoacoustic microscopy and computed tomography," *Nat. Photonics* **3**(9), 503–509 (2009).
10. C. Kim, C. Favazza, and L. H. V. Wang, "*In vivo* photoacoustic tomography of chemicals: high-resolution functional and molecular optical imaging at new depths," *Chem. Rev.* **110**(5), 2756–2782 (2010).
11. L. D. Wang et al., "Video-rate functional photoacoustic microscopy at depths," *J. Biomed. Opt.* **17**(10), 106007 (2012).

12. S. Hu, K. Maslov, and L. V. Wang, "Second-generation optical-resolution photoacoustic microscopy with improved sensitivity and speed," *Opt. Lett.* **36**(7), 1134–1136 (2011).
13. Y. Wang et al., "*In vivo* integrated photoacoustic and confocal microscopy of hemoglobin oxygen saturation and oxygen partial pressure," *Opt. Lett.* **36**(7), 1029–1031 (2011).
14. A. R. Fisher, A. J. Schissler, and J. C. Schotland, "Photoacoustic effect for multiply scattered light," *Phys. Rev. E* **76**(3), 036604 (2007).
15. C. G. Lou and D. Xing, "Photoacoustic measurement of liquid viscosity," *Appl. Phys. Lett.* **96**(21), 211102 (2010).
16. F. Gao et al., "Thermoacoustic resonance effect and circuit modelling of biological tissue," *Appl. Phys. Lett.* **102**(6), 063702 (2013).
17. J. R. Taylor, *Classical Mechanics*, University Science Books, Mill Valley, California (2005).
18. G. D. Gao, S. H. Yang, and D. Xing, "Viscoelasticity imaging of biological tissues with phase-resolved photoacoustic measurement," *Opt. Lett.* **36**(17), 3341–3343 (2011).
19. F. Gao, Y. J. Zheng, and D. F. Wang, "Microwave-acoustic phasoscopy for tissue characterization," *Appl. Phys. Lett.* **101**(4), 043702 (2012).
20. K. Maslov and L. V. Wang, "Photoacoustic imaging of biological tissue with intensity-modulated continuous-wave laser," *J. Biomed. Opt.* **13**(2), 024006 (2008).
21. H. Fang, K. Maslov, and L. V. Wang, "Photoacoustic Doppler effect from flowing small light-absorbing particles," *Phys. Rev. Lett.* **99**(18), 184501 (2007).
22. M. Fatemi and J. F. Greenleaf, "Ultrasound-stimulated vibro-acoustic spectrography," *Science* **280**(5360), 82–85 (1998).
23. R. Muthupillai et al., "Magnetic-resonance elastography by direct visualization of propagating acoustic strain waves," *Science* **269**(5232), 1854–1857 (1995).
24. J. M. Yang et al., "Simultaneous functional photoacoustic and ultrasonic endoscopy of internal organs in vivo," *Nat. Med.* **18**(8), 1297–1302 (2012).
25. S. A. Telenkov and A. Mandelis, "Fourier-domain biophotoacoustic subsurface depth selective amplitude and phase imaging of turbid phantoms and biological tissue," *J. Biomed. Opt.* **11**(4), 044006 (2006).
26. S. Telenkov et al., "Frequency-domain photoacoustic phased array probe for biomedical imaging applications," *Opt. Lett.* **36**(23), 4560–4562 (2011).
27. S. Y. Su and P. C. Li, "Coded excitation for photoacoustic imaging using a high-speed diode laser," *Opt. Express* **19**(2), 1174–1182 (2011).
28. F. Gao, X. H. Feng, and Y. J. Zheng, "Microwave-acoustic correlated imaging and circuit modelling of biological tissues," in *IEEE MTT-S Int. Microwave Workshop Series on RF and Wireless Technologies for Biomedical and Healthcare Applications*, pp. 1–3, IEEE MTTS, Piscataway, New Jersey (2013).
29. F. Gao, Q. Zheng, and Y. J. Zheng, "Electrical circuit modeling and analysis of microwave acoustic interaction with biological tissues," *Med. Phys.* **41**(5), 053302 (2014).

Fei Gao received his BS degree in microelectronics from Xi'an JiaoTong University, Xi'an, China. He has been a PhD student in electrical and electronic engineering at Nanyang Technological University, Singapore, since 2010. His research interests include fundamental study and system development of thermoacoustic and photoacoustic imaging modalities, circuit and system for biomedical applications.

Xiaohua Feng obtained his bachelor's degree in electrical engineering from Xidian University, Xi'an, China, in 2011. He is currently a PhD candidate in the School of Electrical and Electronic Engineering, Nanyang Technological University, Singapore. His research interest includes thermoacoustic imaging, photoacoustic imaging, and pain relief therapy.

Yuanjin Zheng received BEng and MEng degrees from Xi'an Jiaotong University, Xi'an, China, in 1993 and 1996, respectively, and a PhD degree from Nanyang Technological University, Singapore, in 2001. In July 2009, he joined Nanyang Technological University as an assistant professor. His research interests are biomedical sensors and imaging, thermoacoustic and photoacoustic imaging, and SAW/BAW/MEMS sensors. He has authored or coauthored over 100 journal and conference papers, and 16 US patents filed.

Claus-Dieter Ohl received the diplom in physics from the University of Darmstadt (Germany) in 1995 and a PhD in physics in 1999. He did postdocs at Johns Hopkins University (US) in 2000 followed by the University of Twente, The Netherlands. From 2007, he joined Nanyang Technological University in Singapore and was promoted in 2012 to associate professor. His main research interests are experimental fluid mechanics and acoustics, including micro and nanofluidics, cavitation, and interfacial flows.